

Computational Models: 3D Printing, Materials and Structures



Ashish R. Prajapati, Shilpesh R. Rajpurohit,
and Madhukar Somireddy

Abstract A comprehensive understanding of the 3D printing method—microstructure—material properties relationship of 3D printed parts is currently limited. In fused filament fabrication (fused deposition modeling/FDM) 3D printing technology, parts are fabricated by deposition of material layer upon layer. The printing process has a vital influence on the final quality of printed parts. Also, processing parameters control the microstructure of 3D printed components and thus, the parameters in-turn affect the component's material properties. Experimental evaluation of this relationship is challenging, and an alternative solution is computational modeling. The computational models based on multi-physics provide deeper insights into the relationship of process-structure-property of printed parts. This chapter explores different computational models available for modeling the FDM process, computational material models for 3D printed parts and models for characterizing part's material behavior.

1 Introduction

Fused Filament Fabrications (FFF), commonly known as Fused Deposition Modeling (FDM) by Stratasys, is a 3D printing process, which fabricates parts additively. This production process is opposing to traditional machining, where the raw material is cut to get finished parts. The FFF/FDM process is also referred to as material extrusion additive manufacturing (AM) by the community. The FDM process is a versatile advanced fabrication technology among other AM technologies. FDM is commonly used to produce parts with polymeric materials, but the technology can accommodate different materials, including composites, metals,

A. R. Prajapati · S. R. Rajpurohit
Department of Mechanical Engineering, S V National Institute of Technology,
Surat 395007, India

M. Somireddy (✉)
Department of Mechanical Engineering, York University, Toronto, ON M3J 1P3, Canada
e-mail: madhukar@yorku.ca

and ceramics. Furthermore, 3D printers based on this technology are affordable and can fabricate large structures, unlike other AM technologies, which have a limitation on build volume. Such additional benefits with technology increased its demand in many engineering applications. Although the FDM is the most widely used 3D printing technology, but the deeper understanding of the process and its impact on the material properties of final manufactured parts is currently limited. Such challenges can be explored using computational models.

Experimental investigation of parts synthesized via FDM revealed that the printing process has a major effect on the final quality of parts [1]. Mainly, the processing parameters such as extrusion temperature, speed of printing, melt flow rate, and chamber temperature govern the quality extrudates. Furthermore, the bonding strength between the adjacent extrudates also influences the mechanical strength of printed parts [2]. Moreover, the dynamics of melt flow and material deposition play an important role in bond formation [3]. Recently, computational models [4–6] have been in use to understand the printing process and its effect on the material properties of printed components.

The properties of 3D printed specimens are ruled by the microstructure, which in turn is governed by different types of printing process parameters such as layer height, angle of raster, printing direction, print orientation, overlap, infill pattern, and infill density [7–10]. Experimental works [11–13] revealed that the final material properties of 3D printed components are anisotropic, and the reason for that is due to variation in the microstructure due to change in printing parameters while building parts. Computational materials and analytical models [14–17] are available for estimation of material properties and further, these models enable modifying the material characteristics of final 3D printed parts. The results of mechanical testing revealed that the mechanical behavior of 3D printed components is comparable to that of laminates behavior and such printed structures can be handled as composite laminate structures [18]. Therefore, laminate mechanic can be used to depict the mechanical properties of 3D printed structures.

In this chapter, we initially explored different computational models available for modeling of the fused deposition process. Then, analytical and computational models for material modeling were presented for the 3D printed structures. Finally, material models were discussed to depict the mechanical behavior of FDM made parts.

2 Modeling of Material Extrusion Process

Currently, understanding of the process science of FDM process modeling is limited. The models that define the melt dynamics, extrusion technique and bonding between successive material layers are crucial for the development of advanced approaches for different 3D printers. Further, understanding the relationship between processing parameters and mechanical properties of printed parts is crucial in enabling the effective design of parts for manufacturing. Also, the relationship is

critical in producing reliable parts for industrial use and in facilitating more intelligent/smart materials. Key elements of the FDM process include the pinch rolled feed mechanism, liquefier dynamics, extrudate (road or bead) spreading, bonding between extrudates, and temperature of the chamber, substrate, and extrudates. This section analyzes the present state of the art in modeling each of these characteristics of FDM process.

The material extrusion process involves the extrusion of polymeric material through a nozzle and the melt flow, usually at higher rates of shear, and followed by quick cooling. This extrusion process significantly influences the geometry, porosity, and mechanical properties of final components. To understand the influence of the material extrusion process, it requires multi-scale multi-physics models that can include flow behaviour of polymer melt, heat transfer, viscoelastic effect, solidification, and crystallization [4]. The material flow deposition of the printing process can be seen in Fig. 1. The extrusion process can be described by governing equations; conservation of mass, conservation of momentum, and the heat equation, and modeling of the process using these governing equations was discussed in [19–21].

Computational models are available for analysis of liquefier dynamics of the modeling [22–24], and investigation of melt deposition and solidification [25]. The aforementioned computational models also provide insights on the effect of inlet velocity, nozzle diameter, and nozzle angle on the melt flow behaviour of fused deposition modeling. Furthermore, computational fluid dynamics models of the material flow and extrusion process helped to understand the influence of velocity ratio, feed rate, the gap between extruder and substrate on the extrudate, and its shape [26]. Numerical models [27] were also employed to investigate the effect of

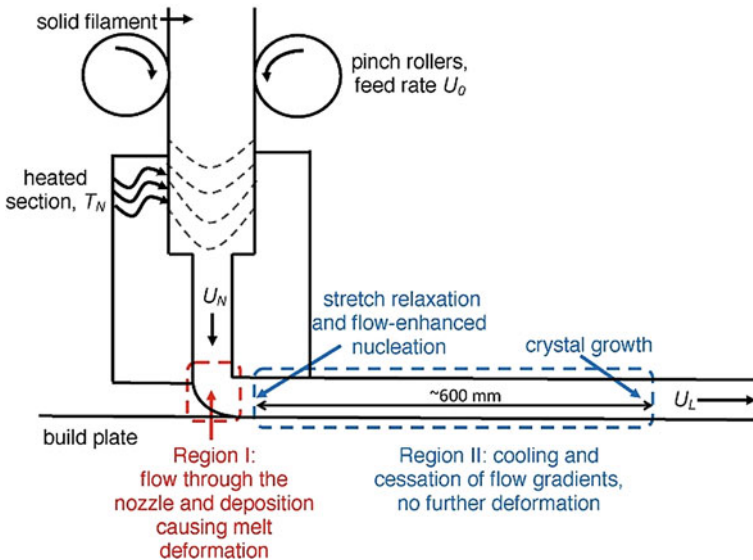


Fig. 1 Material extrusion process of fused deposition modeling [21]

printing speed and layer height on the shape of extrudate. Also, the influence of nozzle speed and nozzle temperature on material deposition was investigated using numerical models [28]. Computational modeling of material deposition also revealed that the deposition rate is greatly influenced by the heat transfer rate [29].

3 Modeling of Bond Formation

The bonding strength between the layers and adjacent extrudates (roads) governs the final strength of 3D printed structures. The bonding strength is ruled by printing process parameters and characteristics of the materials used in printing. In this section, we will see computational models used for simulation for bond formation.

Heat transfer and polymer sintering models were employed to investigate the evolution of neck growth during the formation of the bond [3]. Figure 2 illustrates the bond formation between the adjacent roads, and Fig. 3 shows the same for layers of printed parts. A similar study based on polymer sintering models was also investigated by [5]. The polymer sinter model was used to assess the influence of processing conditions viz. extrusion temperature and the dimensions of the filaments extruded from the nozzle. Extrusion temperature has an important influence on the neck growth between the extrudates and in-turn on the strength of bonding [1].

Thermomechanical simulations revealed that different tool-path patterns cause distortion in the part geometry [30, 31]. The computational model for this is based on three-dimensional transient heat conduction with heat generation due to phase change. A diffusion-controlled healing model was employed to predict the bonding strength between the layers [2]. It revealed that the Z-axis (or inter-layer) strength of 3D printed component depends on printer settings and material properties. In addition, one-dimensional transient thermal analysis of the temperature-dependent diffusion model of the interface between layers was used to predict bond strength.

Thermo-mechanical models [32, 33] were also considered to examine the effects of processing conditions viz. nozzle temperature, speed of the printing, layer height and thermal gradient of synthesized. Thermal analysis was performed to forecast the profile of temperature distribution of a model with similar dimensions of the

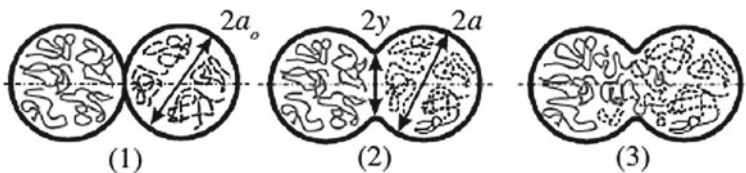
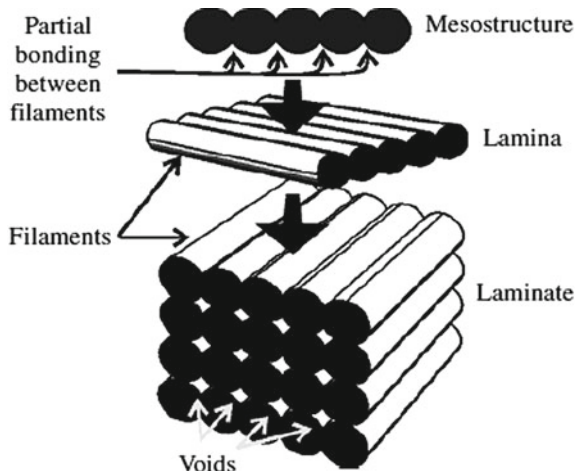


Fig. 2 Bond formation between adjacent extrudates [3] (1) surface contacting, (2) neck growth, (3) diffusion at interface

Fig. 3 Different levels (microstructure to structural level) of 3D printed parts via FDM [3]



part. Also, for the input of analysis, these profiles of temperature distribution were used for thermal stress. Later, it concluded that the developed model could forecast the effective diffusion time with fewer errors than the existing theoretical and numerical models. The numerical model also revealed that low values of temperature, speed of printing, and layer height were helpful for reducing the distortion and residual thermal stresses.

4 Material Modeling of 3D Printed Parts

Anisotropy in the characteristics of 3D printed parts is one of the main concerns for operative design and analysis, as final properties are differing from the properties of the material used for FDM process. This change in the characteristics is primarily because of variation in the mesostructure/microstructure that is built while depositing the material layer upon layer. Material properties are critical for the effective design of structures and consequently, the final properties need to be projected to produce reliable and durable components. The material behavior of 3D printed parts was found to be similar to that of laminate’s behavior [13, 15, 34], and the layers of the specimens can be treated as an orthotropic material. The orthotropic material constitutes nine independent elastic moduli viz. E_1, E_2, E_3 (Young’s modulus), G_{12}, G_{13}, G_{23} (shear modulus) and $\nu_{12}, \nu_{23}, \nu_{13}$ (Poisson’s ratio). Experimental evaluation of nine elastic moduli is challenging and further, it is time consuming and tedious. An alternative to experimental work is analytical methods and computational methods. Constitutive relation of orthotropic material is given as

$$\left\{ \begin{matrix} \sigma_{11} \\ \sigma_{22} \\ \sigma_{33} \\ \tau_{12} \\ \tau_{13} \\ \tau_{23} \end{matrix} \right\} = \begin{bmatrix} C_{11} & C_{12} & C_{13} & 0 & 0 & 0 \\ C_{12} & C_{22} & C_{23} & 0 & 0 & 0 \\ C_{13} & C_{23} & C_{33} & 0 & 0 & 0 \\ 0 & 0 & 0 & C_{44} & 0 & 0 \\ 0 & 0 & 0 & 0 & C_{55} & 0 \\ 0 & 0 & 0 & 0 & 0 & C_{66} \end{bmatrix} \left\{ \begin{matrix} \varepsilon_{11} \\ \varepsilon_{22} \\ \varepsilon_{33} \\ \gamma_{12} \\ \gamma_{13} \\ \gamma_{23} \end{matrix} \right\}, \text{ simply } \{\sigma\} = [C]\{\varepsilon\} \tag{1}$$

$$\{\varepsilon\} = [S]\{\sigma\} \tag{2}$$

Here, compliance matrix is represented by S and different matrix coefficients are:

$$\begin{aligned} S_{11} &= \frac{1}{E_1}, S_{12} = -\frac{\nu_{12}}{E_2}, S_{13} = -\frac{\nu_{13}}{E_1}, S_{22} = \frac{1}{E_2}, S_{23} = -\frac{\nu_{23}}{E_2}, S_{33} = \frac{1}{E_3}, S_{44} \\ &= \frac{1}{G_{12}}, S_{55} = \frac{1}{G_{13}}, S_{66} = \frac{1}{G_{23}} \end{aligned} \tag{3}$$

The components C_{ij} of the C matrix have been found by inverting the compliance matrix. The elastic modulus in the above equation needs to be determined to consider material behavior while designing parts. In this section, we will see different analytical and computational models used in the modeling of FDM made components to estimate the material characteristics.

Rule of mixture: The rule of mixture is the popular and simplest method; this technique is based on the different material mechanics for estimating the overall properties of the composite parts. [15, 35] Mathematical formulation for calculating the overall elastic moduli of 3D printed parts is given below.

$$\bar{E}_1 = (1 - \rho_1)E \tag{4}$$

$$\bar{E}_2 = \bar{E}_3 = \left(1 - \rho_1^{1/2}\right)E \tag{5}$$

$$\bar{G}_{12} = \bar{G}_{13} = G \frac{(1 - \rho_1)(1 - \rho_1^{1/2})}{(1 - \rho_1) + (1 - \rho_1^{1/2})} \tag{6}$$

$$\bar{G}_{23} = \left(1 - \rho_1^{1/2}\right)G \tag{7}$$

$$\bar{\nu}_{12} = \bar{\nu}_{13} = (1 - \rho_1)\nu \tag{8}$$

$$\bar{v}_{13} = \left(1 - \rho_1^{1/2}\right)v \quad (9)$$

$$\bar{v}_{21} = \bar{v}_{31} = \bar{v}_{32} = \left(1 - \rho_1^{1/2}\right)v \quad (10)$$

where, the void density is ρ_1 on first plane in Fig. 4, and E , G and ν are the isotropic properties of the material, which are the elastic properties of the material used for 3D printing. The void density on a plane can be estimated from analysis of the microscopic image of 3D printed part. However, this method can not consider the influence of shape of voids on the properties.

Closed-form orthotropic constitutive model: In this analytical model [37], elastic modulus for a material can be estimated using the following equations. This method accounts for the influence of the void's shape on final material properties. Figure 5 illustrates the unit cell of a 3D printed part with different void shapes.

$$E_{xx} = (1 - f)E \quad (11)$$

$$\nu_{xy} = \nu \quad (12)$$

$$\nu_{xz} = \nu \quad (13)$$

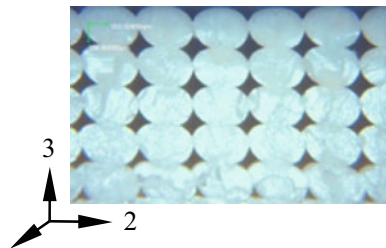
$$\frac{E_{yy}}{E} = \frac{(c - 1)(3c^2 - 1)}{(c - 1)(3c^2 - 1) - f(3c^3 - 3c^2 + c - 3)} \quad (14)$$

$$E_{zz} = E_{yy} \quad (15)$$

$$\nu_{yz} = \frac{\nu(-3c^3 + 3c^2 + c - 1) - f(3c^3 - 3c^2 + c + 1)}{f(3c^3 - 3c^2 + c - 3) - 3c^3 + 3c^2 + c - 1} \quad (16)$$

$$\frac{G_{yz}}{G} = \frac{(c + 1)(1 - 3c^2)}{(c + 1)(1 - 3c^2) + f(\kappa + 1)} \quad (17)$$

Fig. 4 Cross section of 3D printed part [36] (license CC BY 4.0)



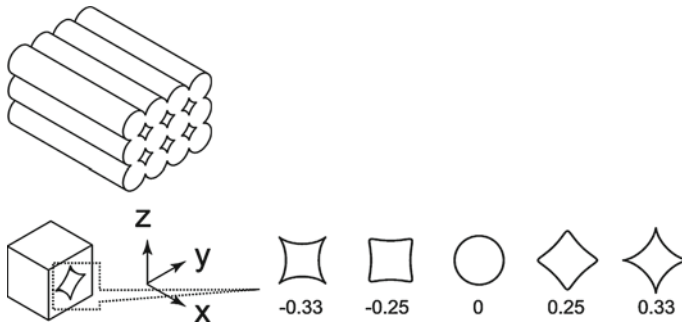


Fig. 5 Unit cell of square array mesostructure [37]

$$\frac{G_{xy}}{G} = \frac{1 - 3c^2}{2f - 3c^2 + 1} \tag{18}$$

$$G_{xz} = G_{xy} \tag{19}$$

Here, mesostructure’s porosity is represented by $f \in [0, 1]$, κ and G are Kolosov constant and shear modulus of the material respectively used for 3D printing. For an isotropic material, the relationship between G , E and ν is written as $G = \frac{E}{2(1+\nu)}$ and $\kappa = \frac{3-\nu}{1+\nu}$. Due to the symmetry of the shape of void, E_{yy} is equivalent to E_{zz} in the closed-form model, and also this model predicts that G_{xy} is equivalent to G_{xz} .

Computational models: In computational methods, the microstructure of FDM made components is used in the FE simulation, and also the material’s properties of the microstructure are considered in the material modeling. The homogenization technique [17, 38, 39] is used for computational material modeling, in this method the unit cell is considered as a homogeneous orthotropic material macroscopically. The fields of the unit cell viz. $\bar{\sigma}_{ij}$ (average stress) and $\bar{\varepsilon}_{ij}$ (average strains) are computed by averaging of the all local stresses σ_{ij} and strains ε_{ij} over the V_{RVE} (volume of RVE) correspondingly. The average stress and strains are written as

$$\bar{\sigma}_{ij} = \frac{1}{V_{RVE}} \int_V \sigma_{ij}(x_1, x_2, x_3) dV \tag{20}$$

$$\bar{\varepsilon}_{ij} = \frac{1}{V_{RVE}} \int_V \varepsilon_{ij}(x_1, x_2, x_3) dV \tag{21}$$

The elastic constitutive relation for a RVE is given as

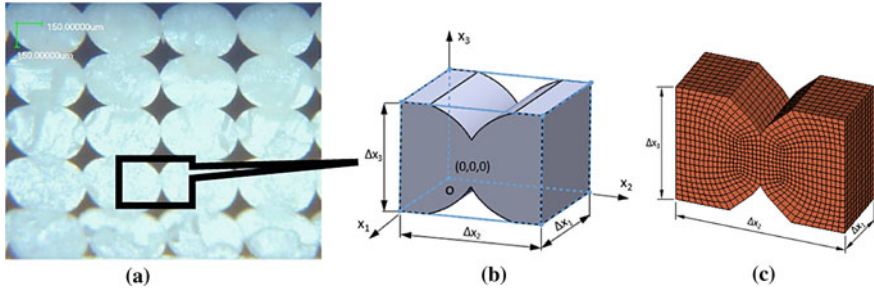


Fig. 6 Microstructure of 3D printed parts [16] **a** unit cell/RVE **b** finite element model

$$\{\bar{\sigma}\} = [C]\{\bar{\epsilon}\} \tag{22}$$

Here, orthotropic material’s constitutive matrix is represented by $[C]$ which is equivalent to $[S]^{-1}$. Then, the strain energy of homogenized RVE can be written as

$$U^* = \frac{1}{2} \{\bar{\epsilon}\}^T [C] \{\bar{\epsilon}\} V_{RVE} \tag{23}$$

The elements which are unknown in the design matrix are obtained with the help of various load conditions. For the deformation model, strain energy (U^*) is calculated using FE simulations and then different values of the stiffness are calculated. Unit cell/RVE plays an important role in determining the properties of FDM made components. Unit cell/RVE is a repetitive architecture of the microstructure of 3D printed parts and it is considered in the homogenization. The RVE is mainly comprised of the material of extrudates and voids between the extrudates, and also their geometry is considered in finite element modeling of RVE. The shape of RVE may vary based on the printing parameters (*e.g.* layer thickness, the orientation of extrudates) used for printing a part. Researchers [16, 17] considered RVE from a single layer of printed parts, refer to Figs. 6 and 7 and on the other hand, RVE is taken from two layers of printed parts [35, 40, 41]. However, these studies treated the RVE as orthotropic material in homogenization.

5 Modeling of Mechanical Behavior of 3D Printed Structures

The material behaviour of FDM made components is similar to the laminate parts [13]. This behaviour is primarily because of the alignment of extrudates (bead or roads) and the deposition of layers while 3D printing. This indicates that the extrudates in a particular printed layer act as a single laminate with several layers acting like a laminated composite part with different orientations of the extrusion.

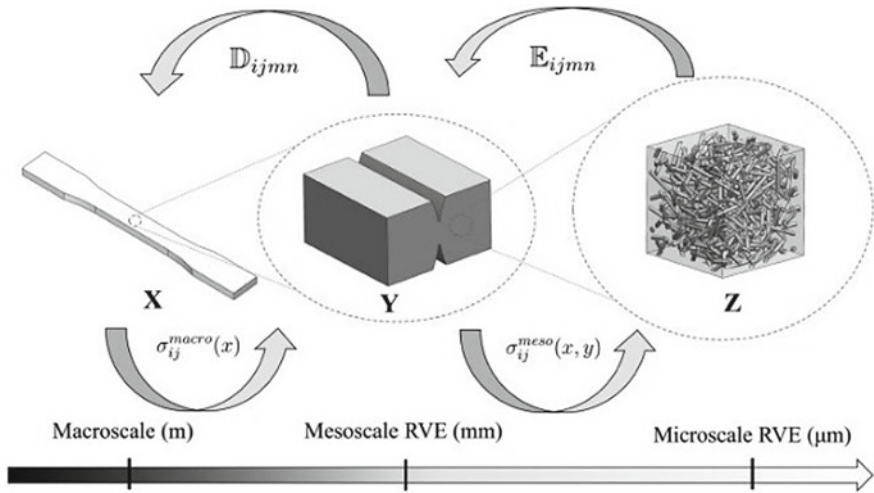


Fig. 7 Three-scale homogenization for 3D printed composite parts [17]

The different layers of the final FDM made part acts like orthogonal anisotropic material and therefore, these can be characterized as a unidirectional fiber reinforced layer. The material behavior of FDM made components can be considered with the help of laminate dynamics and CLT (classical laminate theory) methods. Therefore, CLT helps to characterize the behavior of FDM components that are exposed to various loads during stress analysis. Thus, final FDM made components can be viewed as laminated composite structures that characterize its mechanical behavior.

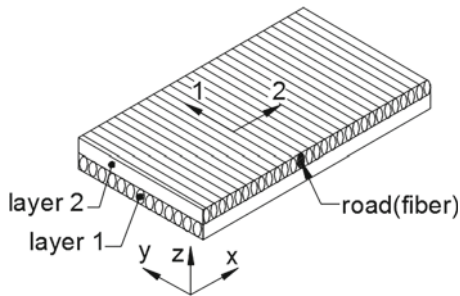
Thin layers of FDM made structures can be characterized with plane stress constitutive relation. Then, for a plane stress case, the constitutive relation of orthotropic materials (Eq. 1) reduces to

$$\begin{Bmatrix} \sigma_{11} \\ \sigma_{22} \\ \tau_{12} \end{Bmatrix} = \begin{bmatrix} Q_{11} & Q_{12} & 0 \\ Q_{12} & Q_{22} & 0 \\ 0 & 0 & Q_{66} \end{bmatrix} \begin{Bmatrix} \varepsilon_{11} \\ \varepsilon_{22} \\ \gamma_{12} \end{Bmatrix} \tag{24}$$

where Q_{ij} components of a constitutive matrix (\mathbf{Q}) of a lamina. The laminate coordinate system is referred to with $x, y,$ and $z,$ and the local coordinate system is denoted with $1, 2,$ and $3,$ as illustrated in Fig. 8.

Classical laminate theory: Figure 8 shows a 3D printed plate with two-layers, with the fibers (extrudates) oriented in layers 1 and 2 at 0° and $90^\circ,$ respectively

Fig. 8 Plate made with FDM in different raster orientation



The displacement field for a lamina from CLT are given as

$$u(x, y, z) = u_0(x, y) + z\phi_x(x, y) \quad (25a)$$

$$v(x, y, z) = v_0(x, y) + z\phi_y(x, y) \quad (25b)$$

$$w(x, y, z) = w_0(x, y) \quad (25c)$$

For a thin layer the rotation terms in Eq. 25 converted into $\phi_x = -\frac{\partial w_0}{\partial x}$, $\phi_y = -\frac{\partial w_0}{\partial y}$, based on the Kirchhoff–Love hypothesis. The strains of the laminate are written as

$$\begin{Bmatrix} \varepsilon_{xx} \\ \varepsilon_{yy} \\ \gamma_{xy} \end{Bmatrix} = \begin{Bmatrix} \varepsilon_{xx}^0 \\ \varepsilon_{yy}^0 \\ \gamma_{xy}^0 \end{Bmatrix} + z \begin{Bmatrix} k_{xx} \\ k_{yy} \\ k_{xy} \end{Bmatrix}, \quad \text{or } \{\varepsilon\} = \{\varepsilon^0\} + z\{k\} \quad (26)$$

where ε_{xx}^0 and ε_{yy}^0 are strains at mid-plane; γ_{xy}^0 is the shear strain; z is the distance from the mid-plane; k_{xx} and k_{yy} are curvatures of bending and k_{xy} is curvature of twisting. The constitutive relation is depicted as:

$$\begin{Bmatrix} \sigma_{xx} \\ \sigma_{yy} \\ \tau_{xy} \end{Bmatrix} = \begin{bmatrix} \bar{Q}_{11} & \bar{Q}_{12} & 0 \\ \bar{Q}_{12} & \bar{Q}_{22} & 0 \\ 0 & 0 & \bar{Q}_{66} \end{bmatrix} \begin{Bmatrix} \varepsilon_{xx} \\ \varepsilon_{yy} \\ \gamma_{xy} \end{Bmatrix}, \quad \text{or } \{\sigma\} = [\bar{Q}]\{\varepsilon\} \quad (27)$$

where \bar{Q}_{ij} are constants of transformed material and the elements of \bar{Q}_{ij} are given as

$$[\bar{Q}] = [T]^{-1}[Q][T]^{-T} \quad (28)$$

Here, $[T]$ is a transformation matrix.

$$[T] = \begin{bmatrix} c^2 & s^2 & 2cs \\ s^2 & c^2 & -2sc \\ -cs & cs & c^2 - s^2 \end{bmatrix} \quad (29)$$

Here, c is $\cos \theta$, s is $\sin \theta$, and θ is the fiber orientation in an counter clockwise direction. The resultant force and moment are defined as

$$\begin{Bmatrix} N_{xx} \\ N_{yy} \\ N_{xy} \end{Bmatrix} = \int_{-h/2}^{h/2} \begin{Bmatrix} \sigma_{xx} \\ \sigma_{yy} \\ \tau_{xy} \end{Bmatrix} dz = \sum_{k=1}^n \int_{h_k}^{h_{k+1}} \begin{Bmatrix} \sigma_{xx} \\ \sigma_{yy} \\ \tau_{xy} \end{Bmatrix}_k dz, \quad \{N\} = \sum_{k=1}^n \int_{h_k}^{h_{k+1}} \{\sigma\} dz \quad (30)$$

$$\begin{Bmatrix} M_{xx} \\ M_{yy} \\ M_{xy} \end{Bmatrix} = \int_{-h/2}^{h/2} \begin{Bmatrix} \sigma_{xx} \\ \sigma_{yy} \\ \tau_{xy} \end{Bmatrix} z dz = \sum_{k=1}^n \int_{h_k}^{h_{k+1}} \begin{Bmatrix} \sigma_{xx} \\ \sigma_{yy} \\ \tau_{xy} \end{Bmatrix}_k z dz, \quad \{M\} = \sum_{k=1}^n \int_{h_k}^{h_{k+1}} \{\sigma\} z dz \quad (31)$$

Using Eqs. 26 and 27, Eqs. 30 and 31 become

$$\{N\} = \sum_{k=1}^n [\bar{Q}] \left[\int_{h_k}^{h_{k+1}} \{\varepsilon^0\} dz + \int_{h_k}^{h_{k+1}} \{k\} z dz \right] = [A]\{\varepsilon^0\} + [B]\{k\} \quad (32)$$

$$\{M\} = \sum_{k=1}^n [\bar{Q}] \left[\int_{h_k}^{h_{k+1}} \{\varepsilon^0\} z dz + \int_{h_k}^{h_{k+1}} \{k\} z^2 dz \right] = [B]\{\varepsilon^0\} + [D]\{k\} \quad (33)$$

Here, N_{xx} and N_{yy} signify the normal forces per unit width; N_{xy} represents the shear force; M_{xx} and M_{yy} represent the bending moments in the y - z and x - z planes, respectively; M_{xy} denotes the twisting moment. $[A]$, $[B]$, and $[D]$ are the stretch stiffness matrix, bond stiffness matrix, and flexural rigidity stiffness matrix, respectively.

$$[A] = \sum_{k=1}^N [\bar{Q}] \int_{h_k}^{h_{k+1}} dz, \quad [B] = \sum_{k=1}^N [\bar{Q}] \int_{h_k}^{h_{k+1}} z dz, \quad [D] = \sum_{k=1}^N [\bar{Q}] \int_{h_k}^{h_{k+1}} z^2 dz \quad (34)$$

The elongation and curvature can be obtained from Eqs. 32 and 33, once the values of normal force and moment are provided. The symmetric laminate structure have the same lamina material properties and fiber orientation evenly distributed above and below the median plane of the laminate. The above mechanics of laminates are useful in characterizing the mechanical behavior of FDM made components under different loadings.

6 Conclusions

Computation models of the extrusion process provided the significance of the different processing parameters on the quality of FDM made structures. The models based on fluid dynamics considered the influence of material flow behavior and the

extrusion process. Polymer sintering models and heat transfer models were employed to investigate the formation of the bonding between the layers, and these models revealed the effects of the temperature of extrusion and chamber environment on the evolution of neck growth. Computational homogenization models were used for material modeling of 3D printed parts, and the final properties of parts were estimated by considering the underlying microstructure of the parts. Finally, the 3D printed parts were treated as laminate structures and the mechanics of laminates were employed to investigate the mechanical behavior of 3D printed parts. In summary, the above computational models provided more insights on the process-structure-property relationship of 3D printed parts, and further, the models were useful to further enhance the quality of parts.

References

1. Sun Q, Rizvi GM, Bellehumeur CT, Gu P (2008) Effect of processing conditions on the bonding quality of FDM polymer filaments. *Rapid Prototyp J* 14(2):72–80
2. Coogan TJ, Kazmer DO (2017) Bond and part strength in fused deposition modeling. *Rapid Prototyp J* 23(2):414–422
3. Bellehumeur C, Li L, Sun Q, Gu P (2004) Modeling of bond formation between polymer filaments in the fused deposition modeling process. *J Manuf Process* 6(2):170–178
4. Das A, McIlroy C, Bortner MJ (2020) Advances in modeling transport phenomena in material–extrusion additive manufacturing: coupling momentum, heat, and mass transfer. *Progress Addit Manuf*. <https://doi.org/10.1007/s40964-020-00137-3>
5. Gurrala PK, Regalla SP (2014) Part strength evolution with bonding between filaments in fused deposition modelling: this paper studies how coalescence of filaments contributes to the strength of final FDM part. *Virtual Phys Prototyp* 9(3):141–149
6. Coogan TJ, Kazmer DO (2017) Healing simulation for bond strength prediction of FDM. *Rapid Prototyp J* 23(3):551–561
7. Tymrak BM, Kreiger M, Pearce JM (2014) Mechanical properties of components fabricated with open-source 3-D printers under realistic environmental conditions. *Mater Des* 58:242–246
8. Huang B, Singamneni S (2015) Raster angle mechanics in fused deposition modelling. *J Compos Mater* 49(3):363–383
9. Cantrell JT, Rohde S, Damiani D, Gurnani R, DiSandro L, Anton J, Young A, Jerez A, Steinbach D, Kroese C, Ifju PG (2017) Experimental characterization of the mechanical properties of 3D-printed ABS and polycarbonate parts. *Rapid Prototyp J* 23(4):811–824
10. Somireddy M, Czekanski A (2020) Anisotropic material behavior of 3D printed composite structures–material extrusion additive manufacturing. *Mater Des* 195:108953
11. Rajpurohit SR, Dave HK (2019) Analysis of tensile strength of a fused filament fabricated PLA part using an open-source 3D printer. *Int J Adv Manuf Technol* 101(5–8):1525–1536
12. Rezayat H, Zhou W, Siriruk A, Penumadu D, Babu SS (2015) Structure–mechanical property relationship in fused deposition modelling. *Mater Sci Technol* 31(8):895–903
13. Somireddy M, Singh CV, Czekanski A (2019) Analysis of the material behavior of 3D printed laminates via FFF. *Exp Mech* 59(6):871–881
14. Ning F, Cong W, Hu Y, Wang H (2017) Additive manufacturing of carbon fiber-reinforced plastic composites using fused deposition modeling: effects of process parameters on tensile properties. *J Compos Mater* 51(4):451–462

15. Li L, Sun Q, Bellehumeur C, Gu P (2002) Composite modeling and analysis for fabrication of FDM prototypes with locally controlled properties. *J Manuf Process* 4(2):129–141
16. Somireddy M, Czekanski A, Singh CV (2018) Development of constitutive material model of 3D printed structure via FDM. *Mater Today Commun* 15:143–152
17. Nasirov A, Gupta A, Hasanov S, Fidan I (2020) Three-scale asymptotic homogenization of short fiber reinforced additively manufactured polymer composites. *Compos B Eng* 202:108269
18. Somireddy M, Singh CV, Czekanski A (2020) Mechanical behaviour of 3D printed composite parts with short carbon fiber reinforcements. *Eng Fail Anal* 107:104232
19. Turner BN, Strong R, Gold SA (2014) A review of melt extrusion additive manufacturing processes: I. Process design and modeling. *Rapid Prototyp J* 20(3):192–204
20. Turner BN, Gold SA (2015) A review of melt extrusion additive manufacturing processes: II. Materials, dimensional accuracy, and surface roughness. *Rapid Prototyp J* 21(3):250–261
21. McLroy C, Graham RS (2018) Modelling flow-enhanced crystallisation during fused filament fabrication of semi-crystalline polymer melts. *Addit Manuf* 24:323–340
22. Bellini A, Güçeri S, Bertoldi M (2004) Liquefier dynamics in fused deposition. *J Manuf Sci Eng Trans ASME* 126:237–246
23. Ramanath HS, Chua CK, Leong KF, Shah KD (2008) Melt flow behaviour of poly- ϵ -caprolactone in fused deposition modelling. *J Mater Sci-Mater Med* 19(7):2541–2550
24. Serdeczny MP, Comminal R, Mollah MT, Pedersen DB, Spangenberg J (2020) Numerical modeling of the polymer flow through the hot-end in filament-based material extrusion additive manufacturing. *Addit Manuf* 36:101454
25. Xia H, Lu J, Dabiri S, Tryggvason G (2018) Fully resolved numerical simulations of fused deposition modeling. Part I: fluid flow. *Rapid Prototyp J* 24(2):463–476
26. Comminal R, Serdeczny MP, Pedersen DB, Spangenberg J (2019) Motion planning and numerical simulation of material deposition at corners in extrusion additive manufacturing. *Addit Manuf* 29:100753
27. Serdeczny MP, Comminal R, Pedersen DB, Spangenberg J (2018) Experimental validation of a numerical model for the strand shape in material extrusion additive manufacturing. *Addit Manuf* 24:145–153
28. Xia H, Lu J, Tryggvason G (2018) Fully resolved numerical simulations of fused deposition modeling. Part II—solidification, residual stresses and modeling of the nozzle. *Rapid Prototyp J* 24(6):973–987
29. Phan DD, Swain ZR, Mackay ME (2018) Rheological and heat transfer effects in fused filament fabrication. *J Rheol* 62(5):1097–1107
30. Zhang Y, Chou YK (2006) Three-dimensional finite element analysis simulations of the fused deposition modelling process. *Proc Inst Mech Eng B J Eng Manuf* 220(10):1663–1671
31. Zhang Y, Chou K (2008) A parametric study of part distortions in fused deposition modelling using three-dimensional finite element analysis. *Proc Inst Mech Eng B J Eng Manuf* 222(8):959–968
32. Zhou Y, Nyberg T, Xiong G, Liu D (2016) Temperature analysis in the fused deposition modeling process. In: 2016 3rd international conference on information science and control engineering (ICISCE) IEEE, pp 678–682
33. Zhou X, Hsieh SJ, Sun Y (2017) Experimental and numerical investigation of the thermal behaviour of polylactic acid during the fused deposition process. *Virtual Phys Prototyp* 12(3):221–233
34. Parandoush P, Lin D (2017) A review on additive manufacturing of polymer-fiber composites. *Compos Struct* 182:36–53
35. Rodríguez JF, Thomas JP, Renaud JE (2003) Mechanical behavior of acrylonitrile butadiene styrene fused deposition materials modeling. *Rapid Prototyp J* 9(4):219–230
36. Somireddy M, Czekanski A (2017) Mechanical characterization of additively manufactured parts by FE modeling of mesostructure. *J Manuf Mater Process* 1(2):18
37. Chen R, Kaplan AF, Senesky DG (2020) Closed-form orthotropic constitutive model for aligned square array mesostructure. *Addit Manuf* 36:101463

38. Yuan Z, Fish J (2008) Toward realization of computational homogenization in practice. *Int J Numer Meth Eng* 73(3):361–380
39. Xia Z, Zhang Y, Ellyin F (2003) A unified periodical boundary conditions for representative volume elements of composites and applications. *Int J Solids Struct* 40(8):1907–1921
40. Anoop MS, Senthil P (2019) Homogenisation of elastic properties in FDM components using microscale RVE numerical analysis. *J Braz Soc Mech Sci Eng* 41(12):540
41. Calneryte D, Barauskas R, Milasiene D, Maskeliunas R, Neciunas A, Ostreika A, Patasius M, Krisciunas A (2018) Multi-scale finite element modeling of 3D printed structures subjected to mechanical loads. *Rapid Prototyp J* 24(1):177–187